Mucosal Mast Cell Secretion Processes Imaged Using Three-Photon Microscopy of 5-Hydroxytryptamine Autofluorescence

Rebecca M. Williams, Jason B. Shear, Warren R. Zipfel, Sudipta Maiti, and Watt W. Webb
School of Applied and Engineering Physics, Cornell University, Ithaca, New York 14853 USA

ABSTRACT The secretion process of the mucosal mast cell line RBL-2H3 was imaged using infrared three photon excitation (3PE) of serotonin (5-hydroxytryptamine, 5-HT) autofluorescence, a measurement previously difficult because of the technical intractability of deep UV optics. Images of prestimulation 5-HT distributions were analyzed in loaded cell populations (those incubated in a 5-HT-rich medium overnight) and in unloaded populations and were found to be strictly quantifiable by comparison with bulk population high-performance liquid chromatography measurements. Antigenically stimulated cells were observed to characteristically ruffle and spread as granular 5-HT disappeared with no detectable granule movement. Individual cells exhibited highly heterogeneous release kinetics, often with quasi-periodic bursts. Neighboring granule disappearances were correlated, indicative of either spatially localized signaling or granule-granule interactions. In one-half of the granule release events, weak residual fluorescence was visible suggestive of leftover 5-HT still bound to the granule matrix. The terminal stages of secretion ($>$300 s) consisted primarily of unresolved granules and remainder 5-HT leakage from already released granules.

INTRODUCTION

The RBL-2H3 mucosal mast cells, in a well-characterized model cell line for the study of hematopoietic signaling and secretion (Oliver et al., 1988) secrete serotonin (5-HT), histamine, and other inflammatory mediators in response to cell-surface IgE-receptor cross-linking by soluble antigen. Although the early biochemical events of this process are being elucidated (Beaven and Metzger, 1993; Field et al., 1995), the mode and mechanism by which secretion occurs are still primarily a mystery. Release assays based on supernatant concentrations of β-hexosaminidase (Schwartz et al., 1979; Tanaka et al., 1991) or radioactive 5-HT ([^{3}H]5-HT) (Seagrave and Oliver, 1990; Weintraub et al., 1994) provide whole population secretion data, allowing the formulation of mechanistic hypotheses. However, by their nature these methods average out an abundant and rich set of cell functions and heterogeneities. Single-cell measurements have shown, for example, that individual cells exhibit signature, patterned, and repeatable calcium oscillations (Millard et al., 1989; Kuchtey and Fewtrell, 1996). In the RBL-2H3 cells, millisecond-resolved amperometric measurements have revealed correlations between these calcium transients and release events (Kim et al., 1997). In chromaffin cells, evidence suggests that release events may be spatially as well as temporally correlated to regions of high calcium entry (Robinson et al., 1995). High-resolution imaging of granules during secretion is critical for a more comprehensive understanding of the mechanism by which secretion occurs. Fluorescent IgE uptake in RBL-2H3 cells (Xu et al., 1998), acridine orange in chromaffin cells (Steyer et al., 1997), and FM-143 in neural cultures (Ryan et al., 1997) have proved successful for loading secretion-competent granules. In addition, other, more targeted methods for specifically tagging the secretory machinery in live cultures are becoming available (Kaether et al., 1997; Miesenbock and Rothman, 1997).

Here we describe imaging measurements of RBL-2H3 secretion, using three-photon excitation (3PE) of 5-HT autofluorescence, a method that possesses both high specificity for identifying secretion-competent granules and an intrinsic 3-D resolution for locating those granules within the cell body (Maiti et al., 1997). The technique is potentially generalizable to analysis of a wide variety of endocrine, epithelial, and neuronal systems. Multiphoton excitation (MPE) of fluorescence is based on the principle that multiple low-energy photons can interact "simultaneously" with a fluorophore and thereby excite an electronic transition of an energy equal to the sum of their combined energies. The application of this nonlinear optical process to laser scanning microscopy (Denk et al., 1990, 1995; Williams et al., 1994; Xu and Webb, 1996; Xu et al., 1996) enables intrinsic 3-D sectioning capabilities without the need for confocal detection optics. Here we utilize low-energy infrared photons (740 nm) and a three-photon mechanism to activate 5-HT autofluorescence, which is normally excited by $<$300 nm illumination (Maiti et al., 1997). 3PE with infrared light alleviates the need for deep UV optics and their associated aberrations and low transmissivities. Furthermore, because MPE is intrinsically localized to the focal plane, it is potentially less invasive than deep UV

Received for publication 2 December 1998 and in final form 11 January 1999.

Address reprint requests to Dr. Rebecca M. Williams, School of Applied and Engineering Physics, Cornell University, Ithaca, NY 14853. Tel.: 607-255-8034; Fax: 607-255-7658; E-mail: rw36@cornell.edu.

Dr. Shear's present address is Department of Chemistry, University of Texas, Austin, TX 78712.

Dr. Maiti's present address is Chemical Physics Group, Tata Institute of Fundamental Research, Kolaba, Mumbai 400005, India.

© 1999 by the Biophysical Society

0006-3495/99/04/1835/12 $2.00

microscopy, which would excite fluorescence throughout the specimen.

It is currently standard practice to image monoamine distributions in fixed tissue using radioactive monoamines (Dave and Kimelberg, 1994), immunohistochemical methods (Wassle and Chun, 1988), or formaldehyde-induced monoamine fluorescence (Falck et al., 1962; Watanabe et al., 1990). However, all of these methods are problematic because of fixation artifacts and are not applicable to live systems. Using one photon excitation with a 305-nm laser line, Lillard et al. have shown that unfixed peritoneal mast cells exhibit fluorescence changes (attributed to 5-HT) upon stimulation (Lillard and Yeung, 1997). In this paper we describe 3PE fluorescence microscopy of granular 5-HT in mucosal mast cells. We show that the technique is quantifiable by comparison with high-performance liquid chromatography (HPLC) and describe what we believe are the first high-resolution images of functional cell processes using monoamine autofluorescence.

MATERIALS AND METHODS

Cell preparation

RBL-2H3 cells are grown in stationary culture and harvested by incubation for 15 min in a calcium chelating buffered salt solution (BSS-): 135 mM NaCl, 5 mM KCl, 20 mM HEPES, and 1.5 mM EDTA (pH 7.4). For the imaging experiments the released cells are centrifuged at 1000 rpm for 8 min, resuspended in the original culture medium, and seeded into 35-mm coverslip-bottom microwells (MatTek Corp.) at 2×10^5 cells/well. Most RBL-2H3 cells express minimal endogenous 5-HT (Weintraub et al., 1994). For some populations (loaded cells), 200 μM of 5-HT (Sigma) is introduced to the culture medium to amplify the granular fluorescence levels. All populations are allowed to adhere overnight at 37°C in a 5% CO_2 incubator. A β-hexosaminidase assay (described below) revealed no significant differences in the population release characteristics (magnitude or time course) as a function of 5-HT loading concentration ($<$1 mM). At 1–2 h before imaging, each well of cells is sensitized with 0.5 μg monoclonal anti-DNP mouse IgE (a gift from the B. Baird Laboratory, Cornell University). Immediately before imaging, cells are rinsed twice and immersed in 1 ml of a HEPES-buffered salt solution (BSS): 135 mM NaCl, 1.8 mM $CaCl_2$, 5 mM KCl, 1 mM $MgCl_2$, 20 mM HEPES, 5 mM glucose, and 0.1% gelatin (pH 7.4). Cells are antigenically stimulated by adding 1 ml of 300 ng/ml DNP-HSA (DNP multiply (30–40) conjugated to human serum albumin; Sigma) in BSS for a final concentration of 150 ng/ml. One milliliter of BSS alone is added as a control "blank" for the unstimulated cells. Most experiments are performed on live cells, but for the fixed population studies, 3.8% paraformaldehyde (Kodak) in a phosphate-buffered saline solution is added to the cells for 10 min. At the 350-nm emission wavelength range used for detection of 5-HT, the autofluorescence of this fixative is negligible. For the HPLC and β-hexosaminidase assays, cells are seeded into 24-well plates at 2×10^5 cells/well and are otherwise treated as in the imaging experiments. To quantify the amounts of 5-HT per cell, the cells are harvested in BSS- and counted with a Coulter cell counter.

HPLC analysis

C_{18} reverse-phase HPLC is performed with an LKB 2150 pump and controller, a Waters Delta Pak column (3.9 $\times$ 150, 5 μm particle size), and a Waters absorbance detector with a 280-nm filter set. By comparison with standards, the minimum 5-HT detection limit is ~5 pmol under these conditions. For the release time course analysis, cells are rinsed twice and stimulated with 200 μl/well of BSS with 150 ng/ml DNP-HSA. The supernatants are removed after varying amounts of time and centrifuged for 5 min at 1200 $\times$ g to remove stray cells. One hundred eighty microliters of the supernatant is then mixed with 20 μl of 30% trichloroacetic acid (TCA) and spun for 2 min at 15,000 $\times$ g to pellet out the protein. The supernatant from this extract is analyzed using a 0.75 ml/min isocratic elution with a solvent designed for separating 5-HT and its oxidative products (Wrona and Dryhurst, 1991): 7% acetonitrile and 0.7% ammonium hydroxide in water, brought to pH 3.2 with formic acid. Cellular extracts are analyzed by harvesting the cells, permeabilizing them with 0.2% TX-100, and proceeding as previously described. 5-HT is quantified by comparing peak areas to a standard curve generated under the same conditions (5-HT in BSS, pelleted with 3% TCA). Under these conditions 5-HT oxidative products (5-hydroxyindole-3-acetic acid and 5,7-dihydroxytryptamine) and other granular constituents (histamine and ATP) are not detected or produce retention times significantly different from those of 5-HT.

β-Hexosaminidase assay

The β-hexosaminidase (β-hex) assay (Schwartz et al., 1979) is performed according to a standard protocol for this cell line (Tanaka et al., 1991). In brief, cells are stimulated to secrete under the same conditions as those in the imaging experiments. Aliquots of supernatant removed at various times are assayed for β-hex activity by incubating them with a β-hex substrate (p-nitrophenyl N-acetyl-β-D-glucosaminide; Sigma) that becomes chromogenic (405 nm) upon cleavage. Absorption measurements indicate differing amounts of β-hex release. All measurements are referenced to the total internal β-hex within each cell population, as determined by permeabilization with 0.2% TX-100.

3PE image acquisition

The 3PE illumination source is provided by an 80-MHz mode-locked, 740-nm beam from an argon-pumped Ti:sapphire laser (Spectra Physics). Pulse widths, measured with a Femtochrome XR-100 autocorrelator, are typically 70–80 fs. The characterized beam is directed in a double pass through two SF-10 prisms (CVI Laser Corp.) to prechirp the pulses in compensation for dispersion effected principally by the microscope objective (Guild et al., 1997). (The prechirp compensation is optimized by maximizing the detected fluorescence from a 3PE test specimen illuminated through the objective.) After the prisms, the beam is attenuated and directed into a retrofitted BioRad MRC-600 confocal scanning box interfaced with a Zeiss Axiovert-35 microscope. A Zeiss 40×/1.3 NA F Fluar objective was chosen for optimal transmission of the ~320–400 nm 5-HT emission. The stage temperature is maintained at 35–37°C with an Airstream stage incubator (Nicholson Precision Instruments) and monitored with an immersion thermocouple (Physitemp).

Because multiphoton excitation is intrinsically localized, confocal detection optics are unnecessary. To avoid signal degradation by extraneous optical elements, the fluorescence is separated from the excitation light by a 400-nm long-pass dichroic mirror (Chroma Technology Corp.) placed between the microscope and the confocal scanner box. It is spectrally filtered with a 2-cm-thick, 1 M $CuSO_4$ solution ($>10^7$ rejection of the 740-nm excitation beam) and a 2-mm-thick piece of UG11 glass ($>10^5$ rejection of 400–600-nm cellular autofluorescence) and detected by a bialkali photomultiplier tube (HC125-02; Hamamatsu). The resulting signal is transmitted through the external junction box to the MRC-600 integrators. The standard BioRad confocal microscopy software is used to acquire and view images.

Cell viability

Of fundamental importance in these studies, as with all live cell imaging, is the determination of experimental conditions in which the cellular processes are not significantly perturbed by the illumination. Excitation

wavelengths and dosages are selected by locating regimes in which both cell spreading (characteristic of antigenic stimulation in this cell line) and granule disappearance are constant and reproducible. Cell viability experiments using Calcein-AM (Molecular Probes) loading as an indicator showed that in the 700–780-nm region with 80–500-fs pulsewidths at 80 MHz, cell viability is limited by two photon cellular absorptions (data not shown). To maximize 3PE processes with respect to the two photon excited processes, the pulsewidth is minimized at the specimen (Xu et al., 1996). This is effected by tuning the laser for the widest uniform and stable spectral spread and by adjusting the compensating prism pair for optimal 3PE fluorescence at the specimen. The use of high NA optics is also critical in the relative accentuation of 3PE processes.

Illumination dosages

Because the 3PE 5-HT absorption cross section is at maximum at 700 nm as compared to other easily accessible wavelengths (Maiti et al., 1997), initial experiments were performed at this excitation wavelength. Although at 700 nm there was no visible damage to the cells, few (~10%) illuminated cells exhibited secretion or secretory morphologies after stimulation. Tuning the wavelength up to 740 nm significantly alleviated this illumination sensitivity. At 740 nm, imaging illumination dosages were reduced until degranulation became constant and reproducible. The live cell image series presented represents data over a total duration of 10–20 min with an average power at the specimen of 5–8 mW, a beam dwell time (beam width (0.17 μm)/beam velocity (0.3 μm/μs)) of 0.6 μs, and an image interval of $\geq$10 s between 1-s image acquisitions. To achieve maximum temporal resolution while minimizing the illumination dosage, data are acquired from a single plane at the granule-rich base of the cells, immediately above the coverslip. The thickness of the optical slice is determined by the axial length of the excitation volume: 0.5 μm full width at half-maximum (Maiti et al., 1997). Three-dimensional data, a series of 15 images at 1-μm intervals, are acquired at the end of each experiment to locate all remaining cellular granules.

Note that all of the time-dependent images are acquired under these low illumination conditions that are nonperturbative to cellular processes. To distinguish all possible detail in static images, acquisition is performed under full illumination: a twofold higher zoom and averaged about five times with the same illumination intensity, yielding a ~10 times higher illumination dose. Under these conditions, cells show no visible signs of damage, but they do not secrete reproducibly. Full illumination images exhibit close to (within 20% of) the ideal diffraction-limited resolution of 0.2 μm (Maiti et al., 1997). Low illumination images, however, are composed of information from few fluorescent photons and thus exhibit an effective resolution that is considerably degraded. Because photons follow Poissonian statistics, the size of the shot noise fluctuations is given by $\sqrt{\langle n \rangle}$, where $\langle n \rangle$ is the average number of photons detected per measurement. Thus to resolve a granular 5-HT concentration to 25% accuracy, at least 16 granule-derived photons must be detected above background. The low illumination imaging conditions described yield only 9 photons/μm^2 (specifically, an average of 1.5 photons/0.16-μm^2 pixel), and thus detail can only be resolved to ~1.4 μm^2.

The static images in Figs. 2 and 7 were acquired using full illumination at the cost of compromising subsequent cellular function. All other data within this paper were derived under low illumination, function-preserving conditions (Fig. 4, for example) and therefore only address spatial scales greater than 1–2 μm. The implications of this limitation are considerable in the discussion of our findings.

Low illumination image analysis

The image data are analyzed by two distinct methods. A pixel distribution analysis of the pixel fluorescence intensities is used to discriminate between fluorescence originating from secretory granules and that of the general cellular matrix. It gives a convenient accounting of average pixel distributions as a function of time. An isocontour analysis of the spatial patterns of pixel intensity is used to identify and locate individual granules, making it possible to inspect granule-specific characteristics automatically.

The pixel distribution analysis for each series of images is accomplished by first determining the basal mean matrix intensity within the cell (μ) and its standard deviation (σ) by averaging 10 regions within cells that (by eye) contain no granules. These values are determined with respect to an extracellular reference level fixed by the image background "black level" (b). Average fluorescence values are calculated by averaging all pixel values greater than b. Pixel distributions throughout the image series are analyzed by defining granule pixels as those possessing values greater than $\mu + 3\sigma$. In a uniform image containing only shot noise deviations, less than 0.3% of pixels would fall above this range (Bevington, 1969).

The isocontour analysis, for individual granule recognition, is accomplished by importing images into the visualization program Data Explorer (DX, IBM). DX is used to smooth each raw image twice with a 5 × 5 Gaussian kernel, an operation that spreads a single variable pixel disturbance to a 3 × 3 pixel (1.4 μm^2) full width at half-maximum, corresponding to the previously described low illumination, shot-noise resolution limit. Isocontours are then constructed around pixels possessing intensities greater than a predetermined excess value above the matrix value μ. In both loaded and unloaded cells, the number of objects thus constructed varies smoothly as a function of the isocontour value used (Fig. 1 *a*). However, in unloaded cells it drops to 0 at an isocontour value just above $\mu + 4\sigma$, whereas in loaded cells discrete objects are still evident at values up to $\mu + 20\sigma$. The isocontour construction value used to recognize granules is determined by the lowest value that results in "0 granule recognition" in images of unloaded cells: $\mu + 5\sigma$. Note that this condition is more stringent than that selected for in the pixel distribution analysis, to avoid tabulating noise-derived objects, which would be disastrous to an object-based (rather than averaging) analysis. The DX isosurface data structure (containing all points and connections) is then assessed to determine areas and centroids of the constructed isocontours. These data are imported into the graphing program SigmaPlot (Jandel Scientific) for further analysis and fitting.

To follow the kinetics of change of individual granule characteristics, isocontours are constructed as previously described on the initial image of each stack, using the image analysis program Alice (Hayden Imaging Group, Perceptive Systems, Inc.). Those particular isocontours clearly deriving from unresolved multiple granules, as assessed by eye, are discarded. The initial area and position of each of these contours is tabulated, and the enclosed average fluorescence is tracked through the image stack by using automated statistics functions within the program. The data are imported into SigmaPlot, with which the fluorescence decrease from each granule as a function of time is fit to a four-parameter logistic function of the form shown in Fig. 1 *b*. The granule release time, Δt, is defined as the time interval required for the granule to drop from 75% to 25% of its releasable fluorescence. The granule release delay, t_0, is defined as the interval between the time that antigen is introduced ($t = 0$) and the time that the granule is half released.

RESULTS

Prestimulation intracellular 5-HT distribution

Previous results have shown that 3PE of 5-HT autofluorescence can be used to identify and characterize 5-HT-loaded secretory vesicles inside RBL-2H3 cells (Maiti et al., 1997). Unloaded cells (Fig. 2 *a*) generally lack punctate features, whereas cells incubated overnight in 200 μM extracellular 5-HT exhibit well-defined and often perinuclear granules (Fig. 2 *b*) emitting a quantity of fluorescence equivalent to that emitted by 50 mM 5-HT (Maiti et al., 1997). An HPLC analysis of lysed cell extracts from loaded cells shows only a single peak, eluted at the characteristic 5-HT retention time. Quantification of the 5-HT peak indicates that loaded

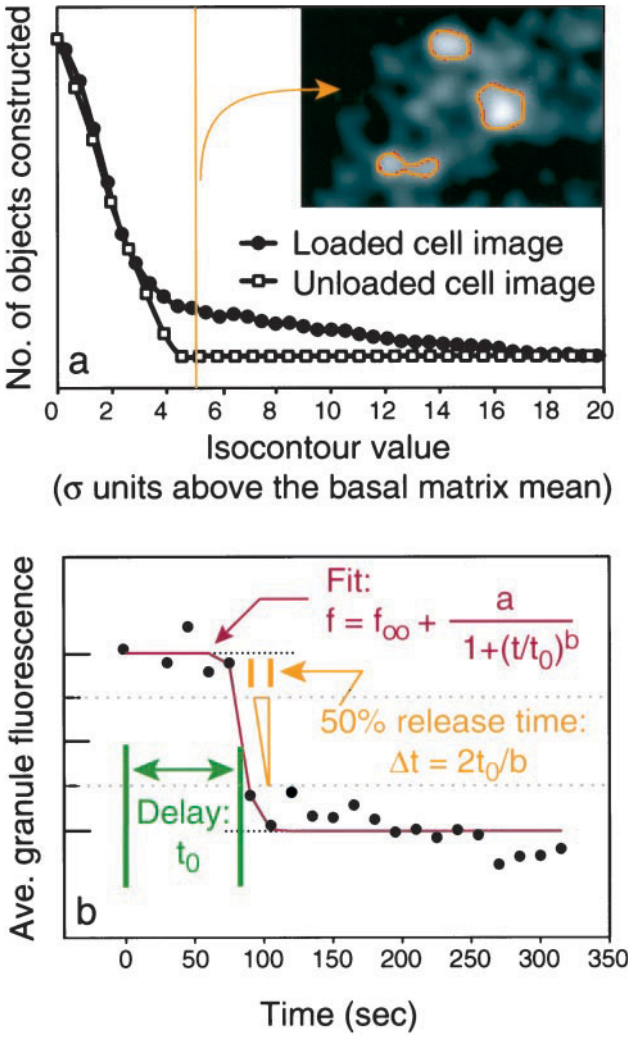

FIGURE 1 Low illumination image analysis for individual granule release kinetics. (*a*) Granules are identified by constructing isocontours around pixels with intensities higher than a "granule recognition" value. The number of objects recognized and constructed in the unloaded cell image (□) falls to 0 at an isocontour value of slightly more than four standard deviations (σ) from the basal fluorescence mean (μ), whereas that in the loaded cell image (●) is nonzero up to $\mu + 20\sigma$. Thus to count the maximum number of granules while ensuring no artifactual ones, a value of $\mu + 5\sigma$ is used for granule identification. The accompanying image shows representative contours (*orange*) constructed by this granule recognition criterion. (*b*) In stimulated cells the average fluorescence within the $\mu + 5\sigma$ isocontour (●) is measured over time and fit to a logistic function (*red equation and curve*). Δt, the 75–25 release time, and t_o, the delay between antigen introduction ($t = 0$) and the time at which half-release has occurred, are extracted from each fit and tallied along with the granule area and its cell of origin.

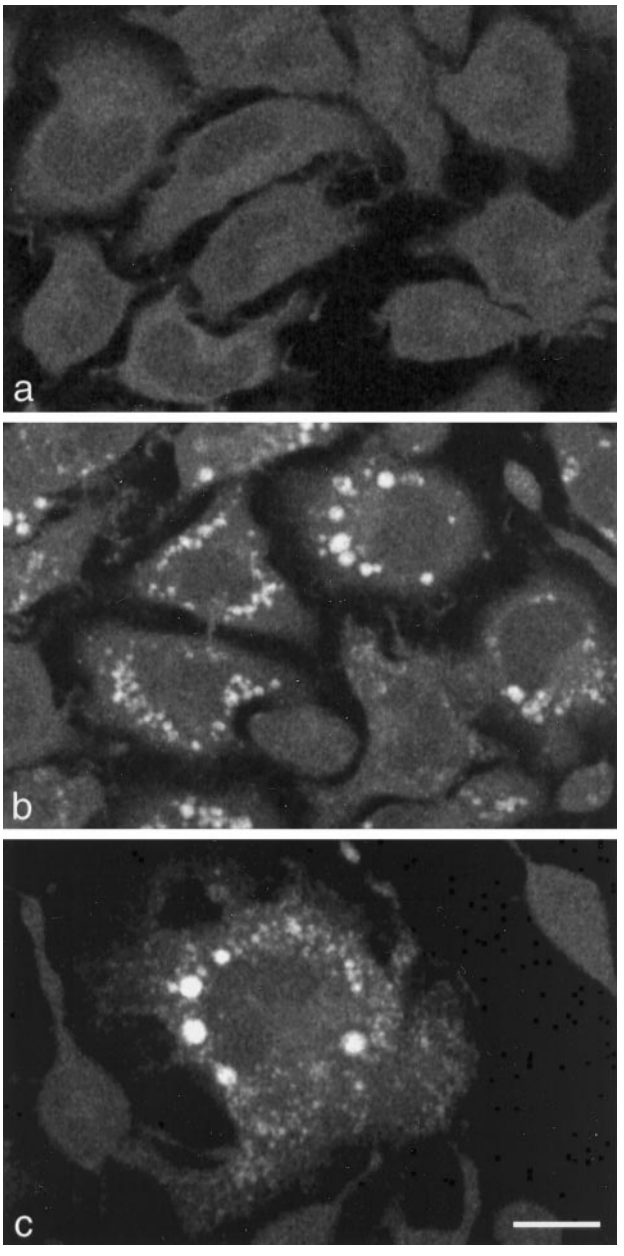

FIGURE 2 Unprocessed 3PE fluorescence images of unloaded and loaded RBL-2H3 cells acquired under full illumination. (*a*) In general, unloaded cells exhibit a modest and relatively uniform fluorescence, which is excluded from the nuclei and slightly enhanced in the Golgi regions, consistent with 3PE of tryptophan-containing proteins. (*b*) Loaded cells, those incubated in a 5-HT-enriched media, accumulate 5-HT in secretion-competent granules by means of 5-HT transporters in the plasma and granule membranes. The basal fluorescence matrix (regions containing no granules by eye) in loaded and unloaded cells is equivalent (within a few percent), indicating that essentially all loaded 5-HT is contained in granules that are resolvable under full illumination. (*c*) A single and unusual (~1%) unloaded cell shows granular fluorescence concentrations similar to those in loaded cells. The scale bar represents 10 μm.

cells contain an average of 1.5 fmol/cell 5-HT, a value that will be shown to be consistent with the 3PE fluorescence imaging measurements.

The basal cellular fluorescence in both loaded and unloaded populations (due to tryptophan-containing proteins, endogenous 5-HT, and any other deep-UV fluorescing compounds) shows a characteristic uniform pattern, excluded by the nuclei and slightly enhanced in the Golgi region. An HPLC analysis of cellular extracts reveals that unloaded cells contain 5% of the 5-HT of loaded cells. The imaging studies of unloaded populations reveal that although most cells contain no granular fluorescence (Fig. 2 *a*), excep-

tional (~1%) unloaded cells (Fig. 2 *c*) contain granules with fluorescence intensities similar to that of the loaded cell population. These cells are typically larger (2–3 times) and are spread thinner than other cells. This granular fluorescence contained within these unusual cells in the unloaded population corresponds to the majority of endogenously expressed 5-HT.

For the described experiments images are acquired under two distinct illumination conditions (see Methods): 1) Full illumination conditions (Figs. 2 and 7) are used for precision imaging under static conditions. These conditions yield a diffraction-limited resolution of ~0.2 μm, but subsequent cellular function is compromised. 2) Low illumination images (all other figures) are necessary for observing secretory dynamics in process. These conditions are nonperturbative to cellular function with repeated imaging but yield a reduced resolution of $> \sim 1$ μm due to photon shot noise.

To test the practical effects of illumination dosage on granule resolution, loaded and unloaded cell populations are compared with both techniques. In full illumination images the basal matrix fluorescence magnitude in unloaded cells is the same (within a few percent) as that in loaded cells, indicating that virtually all of the loaded 5-HT is actually contained within granules resolvable with the high-resolution technique. Measurements acquired under low illumination from prestimulation images reveal an apparent basal fluorescence that is 12% higher in loaded cells as compared to unloaded controls; thus smaller granules are unresolved under these nonperturbing conditions and contribute instead to the apparent basal fluorescence. Quantification of the resolvable granular fluorescence disappearance is accomplished by defining granule pixels as those with values greater than the basal fluorescence mean (μ) by more than 3σ. Stacks of low illumination images at sequential planes throughout the loaded cells reveal that, by this definition, 1% of the total cellular pixels are granular and that the average fluorescence of these granular regions is five times that of the basal fluorescence. These data imply that 5% of the total cellular fluorescence is due to 5-HT in resolved granules, and 12% of the total is due to 5-HT in unresolved granules. Thus only 29% of the loaded 5-HT fluorescence is recognized as resolvable granules under low illumination imaging conditions, although virtually all of the loaded 5-HT is actually associated with detectable granules, as measured with full illumination imaging.

The pixel distribution analysis further yields a measure of the relative volume occupied by granules within cells, which in conjunction with the HPLC analysis provides a check on the 5-HT quantification enabled by multiphoton imaging. Under these loading conditions, granules were previously shown to contain an average 5-HT concentration $C \approx 50$ mM (Maiti et al., 1997). The pixel distribution analysis applied to low illumination images, in which 1% of the cellular volume is resolved as granules, reveals that the granular fluorescence accounts for 29% of the loaded 5-HT. If the total volume of a typical cell is estimated to be $v = 1000$ μ^3 or 1 pl, the total 5-HT per cell (n) should be roughly $n = 3(0.01v)C/0.29 = 1.7$ fmol, a value that agrees to within 15% of our HPLC results.

Stimulated 5-HT release

Instead of performing secretion imaging experiments on the rare unloaded cells exhibiting 5-HT autofluorescence, they are performed on loaded cells because of the resulting vastly improved imaging statistics. Although a β-hex assay shows no significant differences in either the magnitude or time course of secretion in loaded and unloaded cells (data not shown), there may well be functional differences between these two populations that are still undetermined.

On examination of cells at least 12 h after plating, 5-HT-containing granules are found settled primarily at the base of the cells (Fig. 3). (A previous three-dimensional reconstruction (Maiti et al., 1997) shows the more uniform granule distribution expected for shorter times after plating.) Secretion dynamics are imaged within this single granule-rich plane immediately above the coverslip. A three-dimensional stack of images is acquired at the end of each time series to locate all remaining cellular granules. Under low illumination conditions, the granular fluorescence in cells stimulated by exposure to antigen reproducibly disappears, whereas that in control cells exposed only to a buffer "blank" (without antigen) remains essentially constant (Fig. 4). Note that there is the expected characteristic and dramatic change in cellular morphology upon stimulation (Fig. 5). Any abatement of this characteristic cellular spreading and ruffling, a good indication of cellular perturbation, is not observed under low illumination conditions. These and other controls (see Methods) indicate that multiphoton mi-

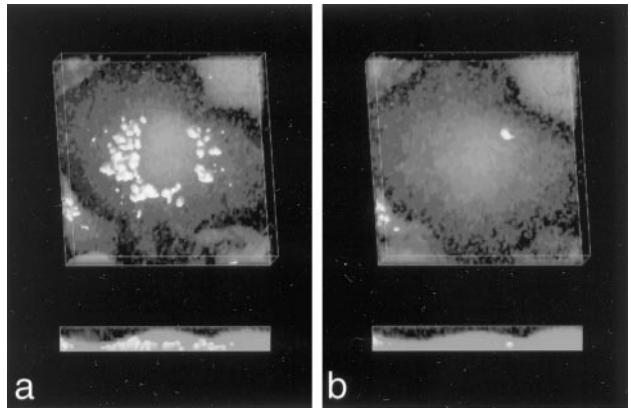

FIGURE 3 Top and side 3-D reconstructions from low-illumination images of a cell initially containing numerous granules (*a*) before and (*b*) 10 min after antigenic stimulation. The RBL-2H3 cells, a mucosal mast cell line, are stimulated to degranulate by cross-linking cell surface IgE receptors by using soluble antigen. Initially the granules lie near the nucleus and at the base of the cell. Upon stimulation the granules disappear, and cell spreading is evident. For each reconstruction data are composed of 15 lateral images at 1-μm steps through the cell. The opaque granule shells are constructed by clamping an isosurface five standard deviations from the basal fluorescence mean (Fig. 1), and the gray values represent a volumetric projection of the full data set.

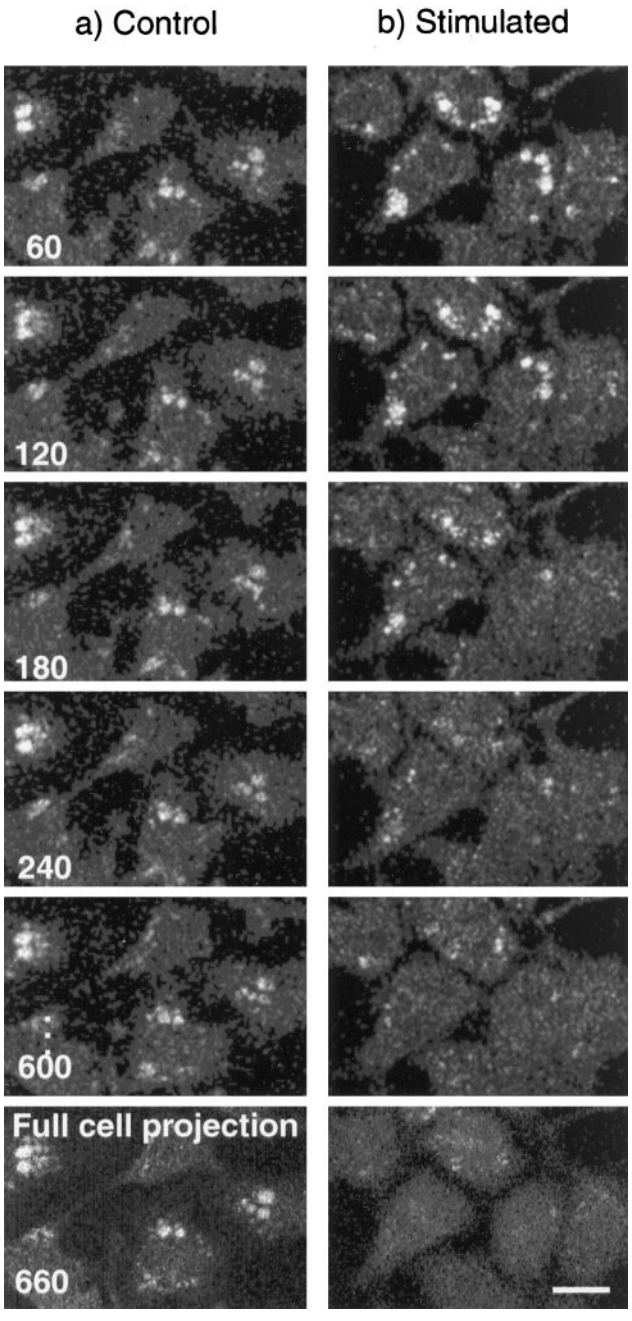

FIGURE 4 3PE fluorescence image time series of 5-HT-loaded cells. Images are acquired at 20-s intervals, but for visual clarity only every third frame is displayed. (*a*) Cells perfused only with buffer remain essentially unchanged, whereas (*b*) those perfused with antigen exhibit a morphological spreading and granule disappearance. For secretion to occur reproducibly, these images are acquired under low (photon-limited) illumination. The resulting signal-to-noise characteristics yield an effective resolution of ~1 μm. (Compare these images to those in Fig. 2, taken with full illumination.) The through-cell projections (last frames) are derived from a 3-D image stack (15 images at 1-μm steps) and show all remaining granules within the cells. The scale bar is 10 μm.

croscopy can be used to functionally probe the dynamics of 5-HT secretion.

In image planes at the base of loaded cells, where granules are most abundant, granular fluorescence accounts for 15% of the total cellular fluorescence (rather than 5% throughout the whole cell, as described earlier). At this plane loaded 5-HT thus accounts for 27% of the total 340-nm fluorescence (15% resolved granular and 12% unresolved granular). An average over 10 experiments with ~30 cells each reveals that during secretion the relative number of granule pixels within stimulated cells declines by 35% and plateaus within 5 min (Fig. 6 *a*), whereas that within unstimulated control cells remains relatively constant. The time scale of this resolved granule fluorescence release is generally about five times faster than that measured for this particular population (data not shown) and for other RBL-2H3 populations (Weintraub et al., 1994; Xu et al., 1998) with either HPLC (quantifying released 5-HT) or β-hex (quantifying released β-hexosaminidase) secretion assays. This apparent temporal discrepancy between the imaging and bulk population secretion measurements suggests the existence of two separate secretion mechanisms, a precept that will be examined further in the Discussion.

Note that cell populations fixed 300 s after stimulation and imaged with full illumination contain essentially no larger granules (>1 μm), as expected by the live cell imaging experiments, but still possess many smaller granules (Fig. 7). These lesser granules indicate leftover and potentially still releasable 5-HT that would not be resolvable under low, nonperturbing illumination. The only systematic exception occurs in mitotic cells, which are known to be unresponsive to applied antigen (Oliver et al., 1988). Mitotic cells, identified by their round morphologies and linear chromatin shadows (Fig. 7 *b, upper right*), still possess large granules 300 s after stimulation, an expected observation for cells that load normally but do not secrete upon exposure to antigen.

In principle, the average cellular fluorescence of 5-HT-loaded cells might be considered to provide a sensitive measure of total secretory release kinetics. The average cellular fluorescence of stimulated cells does decrease along with the granular fluorescence disappearance at shorter time scales ($>$ 300 s), indicating an absolute decrease in cellular fluorescence. However, at longer time scales the morphological changes that accompany cell secretion cause an artifactual increase in these single optical plane measurements. Within the image plane the nuclei, which exclude fluorescence, consist of a decreasing proportion of each cell image as the cells spread along the substrate after activation. Unfortunately, this geometrical effect nullifies the use of average cellular fluorescence as a dynamical measurement approach.

To ensure that the fast granule disappearance is not due either to an illumination-induced acceleration of the release rate or to a net granule movement out of the optical plane, we acquire a full *z*-series of fixed cell populations before and 300 s after antigen introduction. We find that in the stimulated population the total granular fluorescence per cell drops by 35 $\pm$ 11%, a value that is consistent with the granular fluorescence decrease measured in the live cell studies (Fig. 6 *a*). The ability to reproducibly monitor sub-

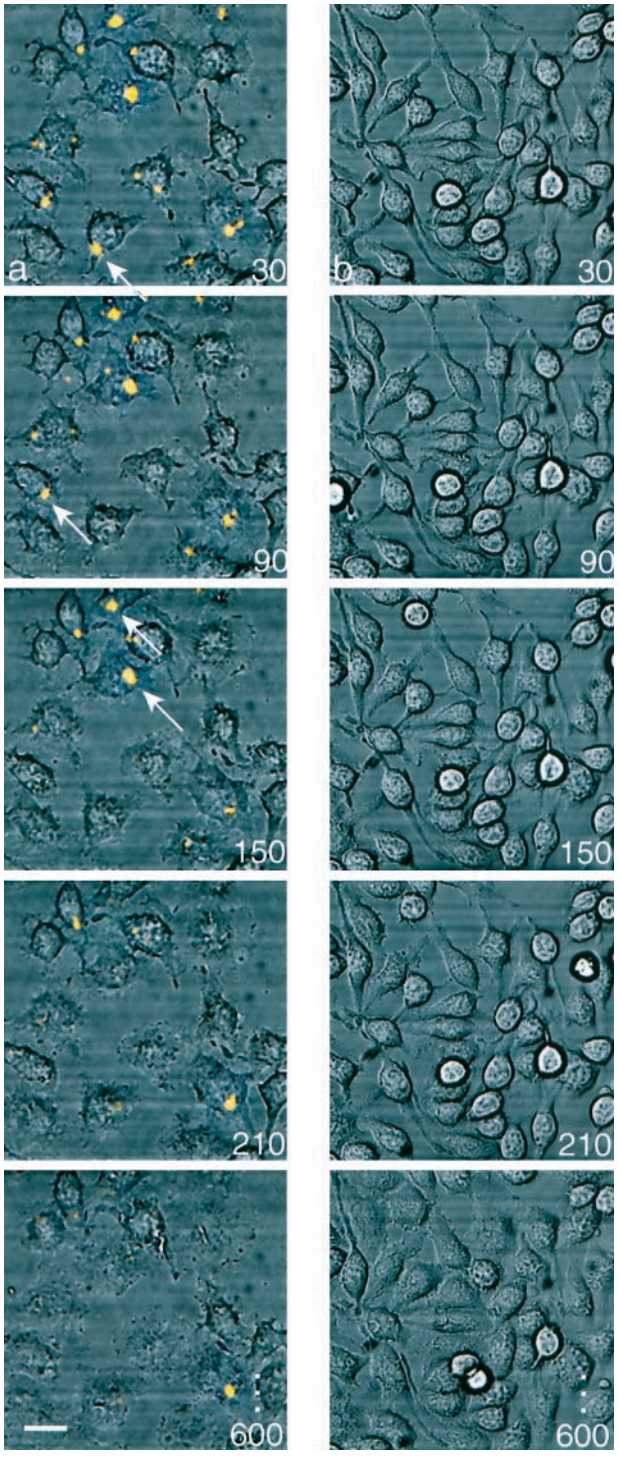

FIGURE 5 Laser scanning transmitted light image series of secreting populations using (*a*) the previously described low-illumination imaging conditions and (*b*) continuous wave (not mode-locked) illumination with a 10-fold reduced power, so that essentially no multiphoton excitations occur. The yellow overlay consists of fluorescence regions corresponding to the $\mu + 5\sigma$ granule recognition criteria (see Methods). Images are acquired every 15 s, but only every fourth frame is displayed here. The degree of ruffling and spreading in response to applied antigen is highly variable within any population. However, under both imaging conditions, the cell morphology changes are dramatic. By 10 min membrane ruffles are abundant and cells have spread to near-confluence. Most of the resolvable granular fluorescence has disappeared within 300 s, when the morphological changes have just begun. The scale bar represents 15 μm.

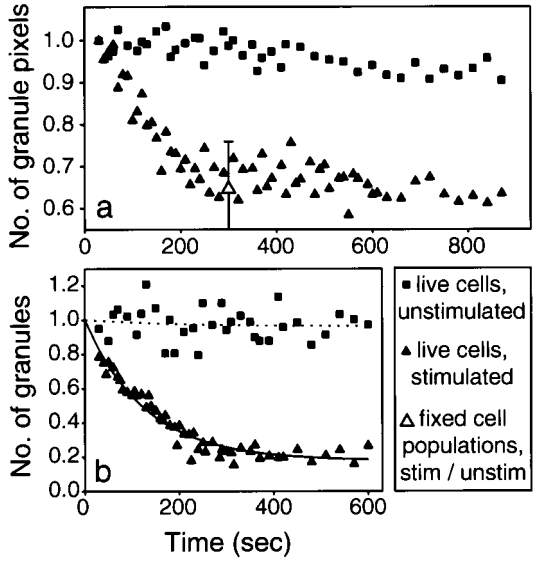

FIGURE 6 Accumulated data from multiple stacks of image series. The data are derived from the accumulation of 10 stimulated (▲) and three unstimulated (■) time series of images (see Fig. 4 for an example) with variable (10–30-s) frame intervals and representing a total of ~300 cells. (*a*) Time dependence of granule pixel survival. In stimulated cells the number of granule pixels decreases by 35% and plateaus within 300 s, whereas in unstimulated cells it remains relatively constant. Image stacks through fixed cell populations before and 300 s after antigen introduction yield consistent results. The percentage of granular pixels per cell in stimulated cells drops by 35 ± 11% relative to the unstimulated population (△). (*b*) Time dependence of granule count. Using the same live cell experimental data, a time variable tally of granules, identified according to an isocontour analysis, shows similar release kinetics. The granule release rate of stimulated cells during the first 300 s is fit by a release rate of 8×10^{-3} s^{-1}.

cellularly resolved and changing 5-HT distributions within these cells enables further investigation of some mechanistic aspects of secretion that are unmeasurable with static or whole population analyses.

Granule release characteristics

To begin to examine individual granule behavior and correlations, a granule recognition protocol was developed. An accounting of objects constructed using this isocontour analysis (see Methods) yields degranulation kinetics similar to those obtained with the pixel distribution analysis (Fig. 6 *b*). Tracking granule centroids through image time series reveals that granules from stimulated cells (before they disappear) show no significant movement above the ~1-μm resolution limitations associated with low illumination imaging conditions (data not shown). Individual granule fluorescence changes can thus be followed by extracting the variable enclosed fluorescence within a fixed isocontour boundary determined in the initial image.

In Fig. 8 *a* the red, orange, and green symbols represent the average fluorescence contained within different granules from several color-coded cells. For the granules resolved under low illumination conditions, no correlations are evi-

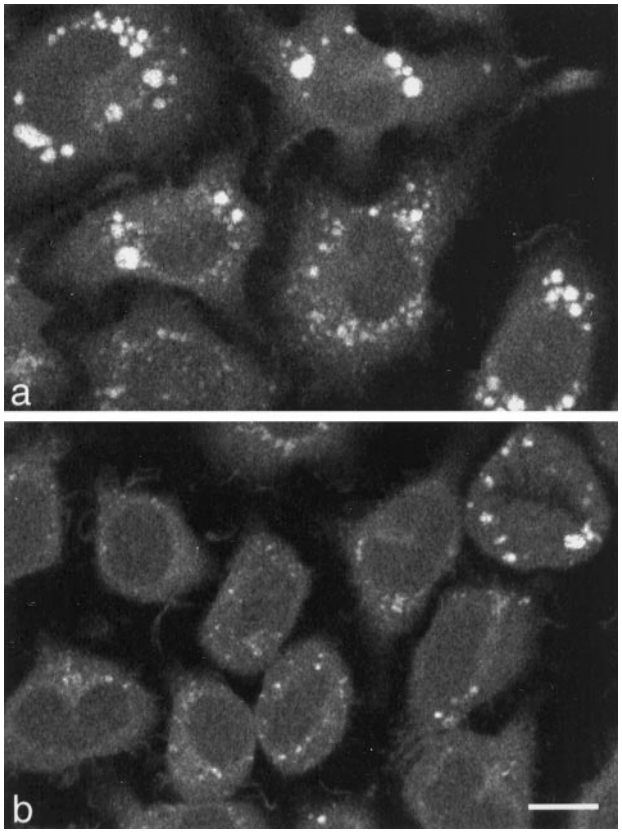

FIGURE 7 Full illumination images from fixed cell populations (*a*) before and (*b*) 300 s after application of antigen. Large granules are prevalent in the unstimulated population but rare in the stimulated population. Mitotic cells like that in the upper right of *b* present a general exception to this rule. These cells contain large granules even after stimulation and are in fact known to be unresponsive to antigenic stimulation (Oliver et al., 1988).

dent between the initial granule characteristics—their size or fluorescence magnitude—and their respective release characteristics. Individual cells, however, exhibit highly heterogeneous release characteristics. The red cell shows highly correlated sudden release, whereas the orange and green cells show slower release with multiple characteristic release times. The distribution of granule release times (Δt's) is plotted in Fig. 8 *b*. A statistical analysis of this behavioral diversity of cell-specific granules shows that it is far greater than random variation. A Student's *F*-test of the granule release slopes reveals that fully 70% of granules analyzed as particular cell populations are statistically different (99.9% confidence interval) from the random distribution as analyzed over the whole granule population. Release delays (t_0's) from single cells are also bunched (Fig. 8 *c*), but often at several characteristic release times, suggestive of bursts of release from individual cells. Quasiperiodic release is more clearly evident in cells with many granules, such as that shown in Fig. 9 *b*.

Fig. 9 shows an example of cell-specific and granule-specific release time courses selected to represent characteristics prevalent in the secretion dynamics observed. Within cells containing multiple granules, release events are not only temporally correlated but frequently regionally correlated as well. In Fig. 9 *a*, multiple granules disappear first at the upper left area of the cell and later at the lower right. In these many-granuled cells, the release is usually somewhat periodic with a time scale of 1–2 min, as is evident in the average time course displayed below. The image series detail in Fig. 9 *b* shows the time course of a single granule release event. Granule contents are observed to disappear with no significant granule movement. In the corresponding graph, the fluorescence from all identified granules within this particular image series are plotted for comparison. Often residual granule footprints are observed, with up to 30% of the granule contents remaining inside a clearly distinguishable granule (see *orange trace*, which corresponds to the displayed image series detail). Of the 200 released granules analyzed, 52% display residual fluorescence (>20% above the basal matrix mean) after release. Sevety-three percent of these residual granules show a gradual (minutes in duration) fluorescence leakage after the initial fast release (*green trace*, for example). These decreases can significantly exceed the 10–20% decreases attributable to photobleaching (see the *black* nonreleasing granule trace in Fig. 9 *b* or the granule pixel decline for unstimulated cells in Fig. 6 *a*). They indicate that many granule interiors are at least transiently accessible to the extracellular environment for extended periods of time after release.

DISCUSSION

Because 3PE of the normally deep-UV absorbing 5-HT is confined to the focal plane, it may be less invasive than conventional linear excitation at <300-nm wavelengths. Using 3PE microscopy of loaded 5-HT autofluorescence, we are able to locate, characterize, and follow functional secretory granules in RBL-2H3 cells. Although reduced illumination intensity at a single focused plane within the cells is necessary to avoid perturbation of cellular function during kinetic studies, subsequent *z*-series and high-resolution images of fixed secreting populations confirm the structural interpretation of the kinetics results. Upon antigenic stimulation the cells spread along the substrate, and within minutes (median t_0 = 84 s) the autofluorescent 5-HT contents within resolvable granules disappear (median Δt = 29 s), with no associated granule motion. The overall kinetics of cellular secretion can be expressed as a fast release from individual large granules (comprising less than a third of the total loaded 5-HT) superimposed upon a slower release of smaller granules and leakages of granule residues.

Mechanism of granular contents transport

Granule transport is not observed; that is, the amount of granule movement in stimulated cells (before release) is small compared to micron-sized resolution limitations in-

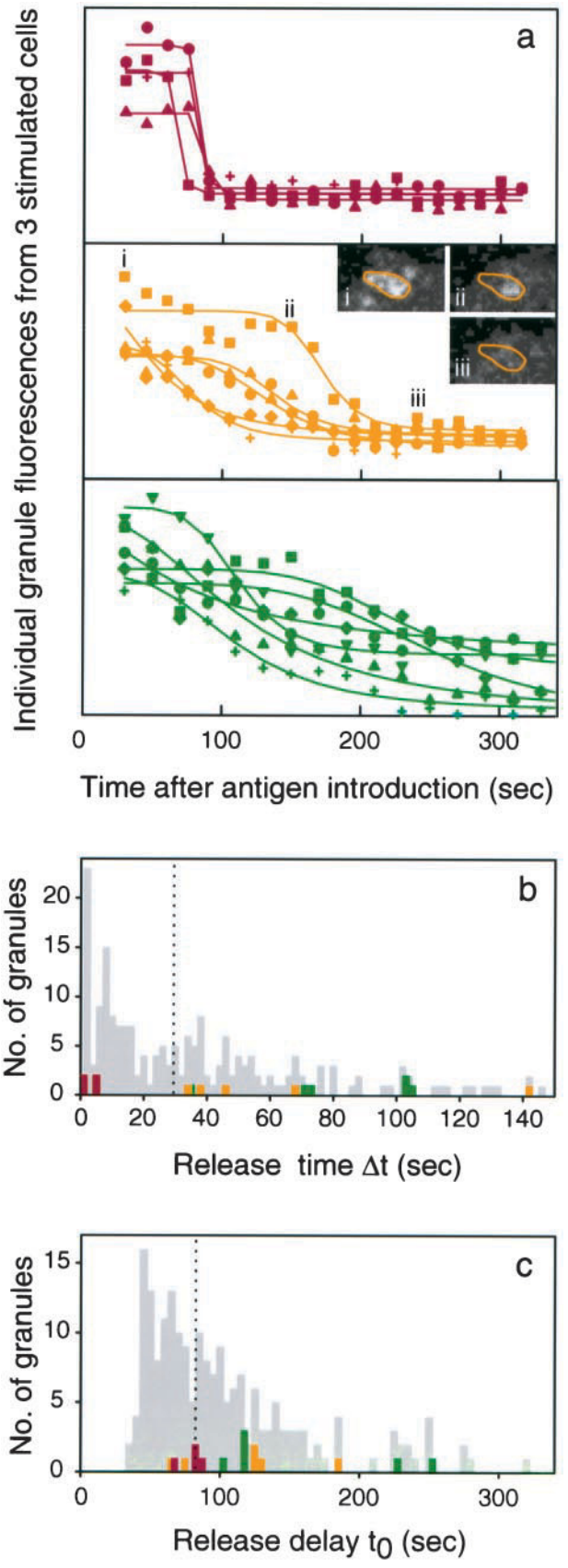

FIGURE 8 Granule-specific release characteristics. (*a*) The average fluorescence from individual granules within several multiple-granuled cells (color-coded by *red*, *orange*, and *green*) are plotted (*symbols*) along with their logistic decrease fits (*lines*). The images associated with the square-coded granule in the orange cell show that the isocontour analysis is sometimes insufficient for distinguishing multiple granules. The fluorescence shows a biphasic release that is clearly the result of two associated but separate granules. In this case the fit only reports the second release event. (*b,c*) Histograms showing the distribution of 200 granule (*b*) release times and (*c*) release delays. The dotted vertical lines correspond to median values for the two distributions, $\Delta t = 29$ s and $t_0 = 84$ s, respectively. The colored bars represent contributions from the single cells above. A Student's *t*-test analysis reveals a significant heterogeneity in the distribution of granule release times from cell to cell; within a given cell, all of the granules (once started) release with similar characteristic speeds. The release delays within the same given cell tend to be more widely distributed and somewhat periodic.

herent in reduced illumination (nonperturbing) imaging. Intracellular movement of whole large granules would be energetically costly, as most estimates for the intracellular "microtrabecular lattice" pore sizes are ~20–100 nm (Gershon et al., 1985; Luby-Phelps et al., 1986). Because (after extended plating) the majority of large granules are settled at the base of the cells, near the basal membrane only, presumably the granular contents are secreted into the substrate/cell interface region or the granular compartments become accessible to other surfaces through interlocking chambers, as observed in classic anaphylactic or global mast cell degranulation (Dvorak, 1995). Stimulated granule-granule fusion, termed *cumulative fusion* or *compound exocytosis*, previously demonstrated in eosinophils with patch-clamp capacitance measurements (Scepek and Lindau, 1993; Hartmann et al., 1995), is consistent with our observations of regionally correlated secretion events.

Correlated release events may also indicate the involvement of spatially localized signaling processes within the cells. Regionally localized calcium transients have not yet been observed in these cells. However, the calcium oscillations previously characterized in the RBL-2H3 line are highly heterogeneous from cell to cell and periodic with a 1–2-min time course (Millard et al., 1989; Kuchtey and Fewtrell, 1996), similar to our observed exocytotic bursts in multiple-granuled cells. Furthermore, simultaneous electrochemical and fluorescent calcium indicator measurements have demonstrated that oscillations of calcium and bursts of exocytotic activity occur concurrently (Kim et al., 1997).

Time scale of secretion

3PE microscopy of granular 5-HT yields a granule release rate that is five times faster than that measured with bulk population 5-HT or β-hexosaminidase assays. However, under function-preserving low illumination conditions, the imaging analysis only resolves a subset of granules; those granules that are small or contain low levels of residual 5-HT appear as basal matrix contributions in the analysis. The imaging analysis thus suggests a duel time course for secretion: a few minutes after activation, the large resolvable granules, residing initially at the base of cells in close

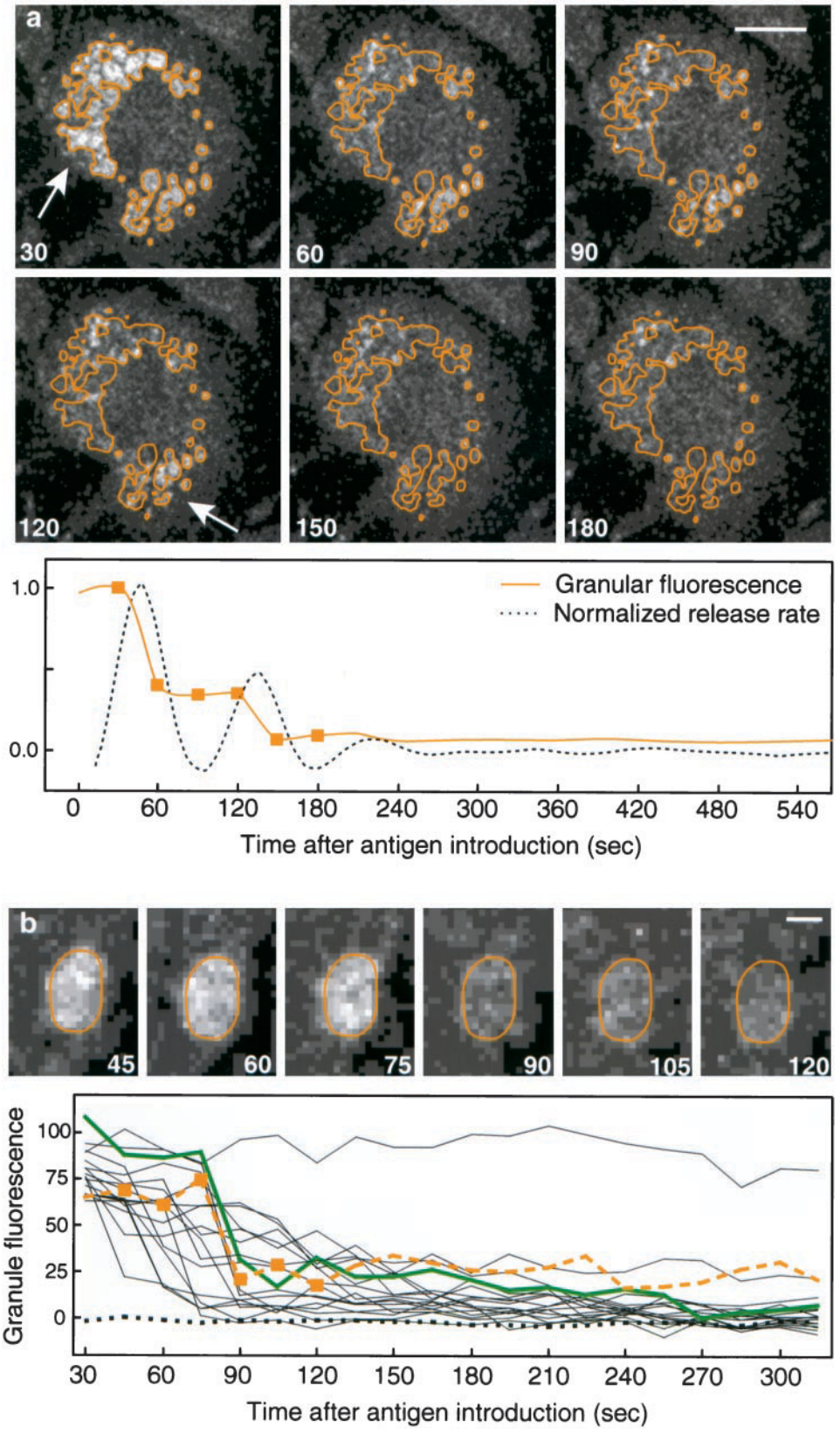

FIGURE 9 Characteristic release attributes at the cell and granule levels. (*a*) An image series in a particularly well-endowed cell shows spatially correlated release events, in which multiple granules disappear first at the upper left and later at the lower right. The average granular fluorescence enclosed by the initial isocontour (*orange*) is plotted below as a function of time (*orange line with squares corresponding to the frames above*). A normalized individual cell release rate (*dotted line*) is calculated using the slope of the granular fluorescence plot. Secretion appears to be oscillatory, with a time scale of ~90 s. The scale bar is 10 μm. (*B*) About one-half of the granules show significant residual fluorescence after release. An example release event is shown in the image series detail, in which the orange isocontour is constructed from the initial smoothed image. Below-average granular fluorescences from all granules within this image series (of which only on granule is shown) are plotted as a function of time. The orange trace (corresponding to the image series detail) shows that the residual fluorescence can account for a significant fraction of the initial fluorescence (in this case 30%). Sevety-three percent of residual granules show a slow fluorescence leakage after an initial fast disappearance (*green trace*, for example). Within this particular field of view, one granule clearly did not release (*constant black line*), a behavior exhibited by 20% of the granules (see Fig. 6 *b*). The dotted black line corresponds to the average basal fluorescence within the cells; the scale bar represents 2 μm.

proximity to the plasma membrane, release in bursts, whereas the bulk of the serotonin (>70%), initially distributed throughout the cells in small granules, is shown by HPLC measurements to release on the 10-min time scale. Also occurring at this time scale are gross cell morphological changes, cell spreading, and ruffle formation, which

decrease the cell surface/volume ratio and thereby enhance the proximity of distributed 5-HT to the cell surface.

Evidence for a biphasic release mechanism already exists. Under some conditions secretion assays on RBL-2H3 populations show clear biphasic behavior (Seagrave and Oliver, 1990; Xu et al., 1998), exhibiting a leveling off at 300 s similar to our own resolvable granule data. In other hematopoietic cells the larger granules are known to possess a distinctly lysozomal character and a pharmacologically distinguishable mechanism of release (Bonifacino et al., 1989; Fittschen and Henson, 1994). Electron micrographs of secreting tissue mast cells and basophils reveal that anaphylactic or global degranulation often coexists with a subsequent piecemeal or segmental degranulation, characterized by intracellular vesicular trafficking at a slower (tens of minutes) time scale (Dvorak and Kissell, 1991; Dvorak, 1995, 1997; Kaminer et al., 1995). One of the few live cell imaging investigations, of chromaffin cell secretion, showed a similar biphasic release (Steyer et al., 1997). In this study evanescent wave images of the cell surface revealed rapid release of granules proximal to the plasma membrane (~2 min), followed by a slower replenishment (~6 min) and subsequent release from the cell interior.

Nature of the transient granule

Simultaneous patch-clamp and electrochemical measurements in mast cells have indicated that 5-HT is initially bound to a proteoglycan matrix (Toledo et al., 1993; Marszalek et al., 1997). Matrix swelling and cation replacement are necessary for 5-HT solvation. Under these conditions, the measured diffusivity for 5-HT is 100 times less than that in solution (Marszalek et al., 1997). After openning of the fusion pore, the release time scale of 5-HT in micron-sized dense granules is measured to be seconds (Toledo et al., 1993). Our observed fast release events ($<$10 s) are consistent with these measurements but are not fully resolvable within the temporal resolution of the experiments. Our observed granule remainders, evident in one-half of the released granules, are reminiscent of electron micrographs of postsecretion mast cells showing compartmentalized dense material within released granules (Dvorak, 1995; Kaminer et al., 1995). They may be the result of leftover undissolved 5-HT, possibly due to incomplete swelling of the granule matrix. The slow 5-HT leakage observed from 73% of the residual granules (minutes in duration) would not be resolvable with amperometric measurements but constitutes a significant portion of the secreted contents. It remains an interesting challenge to understand the structural and molecular mechanisms that control these postrelease leakage processes.

The authors thank Dr. Dave Holowka and Profs. Barbara Baird and Clare Fewtrell for acting as a generous resource to the RBL world, the Baird laboratory for the provision of well-characterized DNP-IgE, and Prof. Manfred Lindau for a helpful critique of the manuscript. We also acknowledge the National Institutes of Health Parallel Processing Resource for Biomedical Science (Cornell Theory Center) for acting as a Data Explorer repository and support center.

This work was supported and carried out through the facilities of the Developmental Resource for Biophysical Imaging and Opto-electronics funded by the National Institutes of Health (RR04224) and the National Science Foundation (NSF) (BIR9419978). JBS was a NSF Postdoctoral Fellow supported by grant CHE-9403174.

REFERENCES

Beaven, M. A., and H. Metzger. 1993. Signal transduction by Fc receptors: the FcεRI case. *Immunol. Today.* 14:222–226.

Bevington, P. R. 1969. Data Reduction and Error Analysis for the Physical Sciences. McGraw-Hill, New York.

Bonifacino, J. S., L. Yuan, and I. V. Sandoval. 1989. Internalization and recycling to serotonin-containing granules of the 80K intergral membrane protein exposed on the surface of secreting rat basophilic leukaemia cells. *J. Cell Sci.* 92:701–712.

Dave, V., and H. K. Kimelberg. 1994. Na^+-dependent, fluoxetine-sensitive serotonin uptake by astrocytes tissue-printed from rat cerebral cortex. *J. Neurosci.* 14:4972–4986.

Denk, W., D. W. Piston, and W. W. Webb. 1995. Two-photon molecular excitation in laser-scanning microscopy. *In* Handbook of Biological Confocal Microscopy. Plenum Press, New York. 445–458.

Denk, W., J. H. Strickler, and W. W. Webb. 1990. Two-photon laser scanning fluorescence microscopy. *Science.* 248:73–76.

Dvorak, A. M. 1995. Ultrastructural analysis of human mast cells and basophils. *In* Human Basophils and Mast Cells: Biological Aspects. Karger, New York. 1–33.

Dvorak, A. M. 1997. New aspects of mast cell biology. *Int. Arch. Allergy Immunol.* 114:1–9.

Dvorak, A. M., and S. Kissell. 1991. Granule changes of human skin mast cells characteristic of piecemeal degranulation and associated with recovery during wound healing in situ. *J. Leukoc. Biol.* 49:197–210.

Falck, B., N. A. Hillarp, C. Thieme, and A. Torp. 1962. Fluorescence of catechol amines and related compounds condensed with formaldehyde. *J. Histochem. Cytochem.* 10:348–354.

Field, K. A., D. Holowka, and B. Baird. 1995. FcεRI-mediated recruitment of $p53/56^{lyn}$ to detergent-resistant membrane domains accompanies cellular signaling. *Proc. Natl. Acad. Sci. USA.* 92:9201–9205.

Fittschen, C., and P. M. Henson. 1994. Linkage of azurophil granule secretion in neutrophils to chloride ion transport and endosomal transcytosis. *J. Clin. Invest.* 93:247–255.

Gershon, N. D., K. R. Porter, and B. L. Trus. 1985. The cytoplasmic matrix: its volume and surface area and the diffusion of molecules through it. *Proc. Natl. Acad. Sci. USA.* 82:5030–5034.

Guild, J. B., C. Xu, and W. W. Webb. 1997. Measurement of group delay dispersion of high numerical aperture objective lenses using two-photon excited fluorescences. *Appl. Optics.* 36:397–401.

Hartmann, J., S. Scepek, and M. Lindau. 1995. Regulation of granule size in human and horse eosinophils by number of fusion events among unit granules. *J. Physiol. (Lond.).* 483:201–209.

Kaether, C., T. Salm, M. Glombik, W. Almers, and H.-H. Gerdes. 1997. Targeting of green fluorescent protein to neuroendocrine secretory granules: a new tool for real time studies of regulated protein secretion. *Eur. J. Cell Biol.* 74:133–142.

Kaminer, M. S., G. F. Murphy, B. Zweiman, and R. M. Lavker. 1995. Connective tissue mast cells exhibit time-dependent degranulation heterogeneity. *Clin. Diagn. Lab. Immunol.* 2:297–301.

Kim, T. D., G. T. Eddlestone, S. F. Mahmoud, J. Kuchtey, and C. Fewtrell. 1997. Correlating Ca^{2+} responses and secretion in individual RBL-2H3 mucosal mast cells. *J. Biol. Chem.* 272:31225–31229.

Kuchtey, J., and C. Fewtrell. 1996. Subcloning the RBL-2H3 mucosal mast cell line reduces Ca^{2+} response heterogeneity at the single cell level. *J. Cell. Physiol.* 166:643–652.

Lillard, S. J., and E. S. Yeung. 1997. Temporal and spatial monitoring of exocytosis with native fluorescence imaging microscopy. *J. Neurosci. Methods.* 75:103–109.

Luby-Phelps, K., D. L. Taylor, and F. Lanni. 1986. Probing the structure of cytoplasm. *J. Cell Biol.* 102:2015–2022.

Maiti, S., J. B. Shear, R. M. Williams, W. R. Zipfel, and W. W. Webb. 1997. Measuring serotonin distribution in live cells with three-photon excitation. *Science.* 275:530–532.

Marszalek, P. E., B. Farrell, P. Verdugo, and J. M. Fernandez. 1997. Kinetics of release of serotonin from isolated secretory granules. II. Ion exchange determines the diffusivity of serotonin. *Biophys. J.* 73: 1169–1183.

Miesenbock, G., and J. E. Rothman. 1997. Patterns of synaptic activity in neural networks recorded by light emission from synaptolucins. *Proc. Natl. Acad. Sci. USA.* 94:3402–3407.

Millard, P. J., T. A. Ryan, W. W. Webb, and C. Fewtrell. 1989. Immunoglobin E receptor cross-linking induces oscillations in intracellular free ionized calcium in individual tumor mast cells. *J. Biol. Chem.* 264: 19730–19739.

Oliver, J. M., J. Seagrave, R. F. Stump, J. R. Pfeiffer, and G. G. Deanin. 1988. Signal transduction and cellular response in RBL-2H3 mast cells. *Prog. Allergy.* 42:185–245.

Robinson, I. M., J. M. Finnegan, J. R. Monck, R. M. Wrightman, and J. M. Fernandez. 1995. Colocalization of calcium entry and exocytotic release sites in adrenal chromaffin cells. *Proc. Natl. Acad. Sci. USA.* 92: 2474–2478.

Ryan, T. A., H. Reuter, and S. J. Smith. 1997. Optical detection of a quantal presynaptic membrane turnover. *Nature.* 388:478–482.

Scepek, S., and M. Lindau. 1993. Focal exocytosis by eosinophils—compound exocytosis and cumulative fusion. *EMBO J.* 12:1811–1817.

Schwartz, L. B., K. F. Austen, and S. I. Wasserman. 1979. Immunologic release of β-hexosaminidase and β-glucuronidase from purified rat serosal mast cells. *J. Immunol.* 123:1445–1450.

Seagrave, J., and J. M. Oliver. 1990. Antigen-dependent transition of IgE to a detergent-insoluble form is associated with reduced IgE receptor-dependent secretion from RBL-2H3 mast cells. *J. Cell. Physiol.* 144: 128–136.

Steyer, J. A., H. Horstmann, and W. Almers. 1997. Transport, docking and exocytosis of single secretory granules in live chromaffin cells. *Nature.* 388:474–478.

Tanaka, Y., Y. Takagaki, and T. Nishimune. 1991. Effects of metal elements on β-hexosaminidase release from rat basophilic leukemia cells (RBL-2H3). *Chem. Pharm. Bull.* 39:2072–2076.

Toledo, G. A. d., R. Fernandez-Chacon, and J. M. Fernandez. 1993. Release of secretory products during transient vesicle fusion. *Nature.* 363:554–558.

Wassle, H., and M. H. Chun. 1988. Dopaminergic and indoleamine-accumulating amacrine cells express GABA-like immunoreactivity in the cat retina. *J. Neurosci.* 8:3383–3394.

Watanabe, T., T. Morikami, and I. Nagatsu. 1990. Immunohistochemical colocalization of glucagon, serotonin, and aromatic L-amino acid decarboxylase in islet A cells of chicken pancreas. *Cell Tissue Res.* 259: 67–72.

Weintraub, W. H., P. Cleveland-Wolfe, and C. Fewtrell. 1994. Paracrine Ca^{2+} signaling in vitro: serotonin-mediated cell-cell communication in mast cell/smooth muscle cultures. *J. Cell. Physiol.* 160:389–399.

Williams, R. M., D. W. Piston, and W. W. Webb. 1994. Two-photon molecular excitation provides intrinsic 3-dimensional resolution for laser-based microscopy and microphotochemistry. *FASEB J.* 8:804–813.

Wrona, M. Z., and G. Dryhurst. 1991. Interactions of 5-hydroxytryptamine with oxidative enzymes. *Biochem. Pharmacol.* 41:1145–1162.

Xu, C., and W. W. Webb. 1996. Measurement of two-photon excitation cross sections of molecular fluorophores with data from 690 to 1050 nm. *J. Opt. Soc. Am. B.* 13:481–491.

Xu, C., W. Zipfel, J. B. Shear, R. M. Williams, and W. W. Webb. 1996. Multiphoton fluorescence excitaiton: new spectral windows for biological nonlinear microscopy. *Proc. Natl. Acad. Sci. USA.* 93:10763–10768.

Xu, K., R. M. Williams, D. Holowka, and B. Baird. 1998. Stimulated release of fluorescently labeled IgE fragments that efficiently accumulate in secretory granules after endocytosis in RBL-2H3 mast cells. *J. Cell Sci.* 111:2385–2396.